Estimation of Collective Maneuvers through Cooperative Multi-Agent Planning

Jens Schulz, Kira Hirsenkorn, Julian Löchner, Moritz Werling, and Darius Burschka

***Abstract*— In order to determine a cooperative driving strategy, it is beneficial for an autonomous vehicle to incorporate the intended motion of surrounding vehicles within its own motion planning. However, as intentions cannot be measured directly and the motion of multiple vehicles often are highly interdependent, this incorporation has proven challenging. In this paper, the problem of maneuver estimation is addressed, focusing on situations with close interaction between traffic participants. Therefore, we define collective maneuvers based on trajectory homotopy, describing the relative motion of multiple vehicles in a scene. Representing maneuvers by sample trajectories, maneuver-dependent prediction models of the vehicle states can be defined. This allows for a Bayesian estimation of maneuver probabilities given observations of the real motion. The approach is evaluated by simulation in overtaking scenarios with oncoming traffic and merging scenarios at an intersection.**

I. Introduction

Predicting the motion of nearby vehicles is a prerequisite for safe, foresighted, and cooperative driving of autonomous vehicles. As human drivers have individual and highly complex behaviors, prediction will always be afflicted with uncertainty. Thus, it is difficult to derive one accurate deterministic prediction that an autonomous vehicle can rely on for its own motion planning. One alternative to this problem is to consider multiple discrete maneuver hypotheses within the prediction and estimate the probability distribution over them. This maneuver estimate can in turn be used as a basis for a continuous motion prediction.

Especially in situations where decisions of traffic participants are highly coupled, the assumption of independent motion becomes invalid. This motion interdependency of nearby vehicles and the ego-vehicle yields additional challenges, as it is not possible to separate the problems of prediction and planning anymore. This can be seen in Fig. 1 where the black and white vehicle closely interact. Without anticipating the maneuver decision of the other driver, one can hardly decide for one of the two options. However, the own decision may influence the decision of the other driver as well.

In this paper, we approach this problem by defining collective maneuvers on a multi-agent scale, describing the relative motion of multiple vehicles in a scene. As the interconnection of decisions often arise from geometric collision avoidance constraints, the maneuver definition is based on the concept of trajectory homotopy. Cooperative multi-agent trajectories are planned for the given maneuvers to reflect common human behavior. These sample trajectories, used to represent the corresponding maneuvers, allow for a comparison of abstract maneuver classes and observations of the actual motion. Through Bayesian statistic, using an interacting multiple model estimator, the probability distribution over the possible maneuvers is derived, serving as a basis for the decision making of the autonomous vehicle. As the ego-vehicle as well as other vehicles are included in the multi-agent planning process, both tasks, prediction and motion planning, are solved at once. Thus, we overcome the interdependency of prediction and planning, resulting in a cooperatively driving autonomous vehicle.

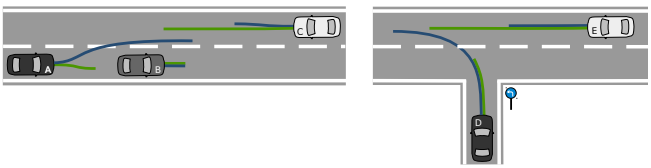

Fig. 1. Two situations where the black and white vehicles' motions are highly coupled. Multi-agent trajectories are shown for two collective maneuver hypotheses (blue and green). Both vehicles should intend to follow the same maneuver for collisions and misunderstandings to be avoided.

Fig. 2 provides an overview of the maneuver estimation and planning framework. The single components are explained in detail within the remaining chapters of this paper: Sec. II summarizes the related work in the area of motion prediction and maneuver representation. The collective maneuvers and how they are derived are described in Sec. III. Sec. IV depicts the multi-agent trajectory planning including the constraints to enforce a specific maneuver class. In Sec. V the maneuver probability distribution is derived given the sample trajectories and the motion observations. Sec. VI evaluates and Sec. VII concludes the presented work.

II. Related Work

In the area of autonomous vehicles, motion prediction of other traffic participants has been widely studied. One component is the estimation of currently conducted or upcoming maneuvers. Commonly, the set of possible maneuvers is defined by hand using expert knowledge. For highway scenarios, this is often done by using discrete lane matchings and distinguishing between different states a vehicle can reside in, as for example *free flow*, *car following*, *lane change* and *overtaking* [1]. A more detailed description has been used by [2], where an overtaking maneuver is compound by a series of behaviors: *acceleration phase*, *sheer out*, *overtake*,

J. Schulz is with BMW Group and the Department of Computer Science, Technical University of Munich, Germany. jens.schulz@bmw.de

K. Hirsenkorn, J. Löchner, and M. Werling are with BMW Group, Munich, Germany. {kira.hirsenkorn | julian.loechner | moritz.werling}@bmw.de

D. Burschka is with the Department of Computer Science, Technical University of Munich, Germany. burschka@tum.de

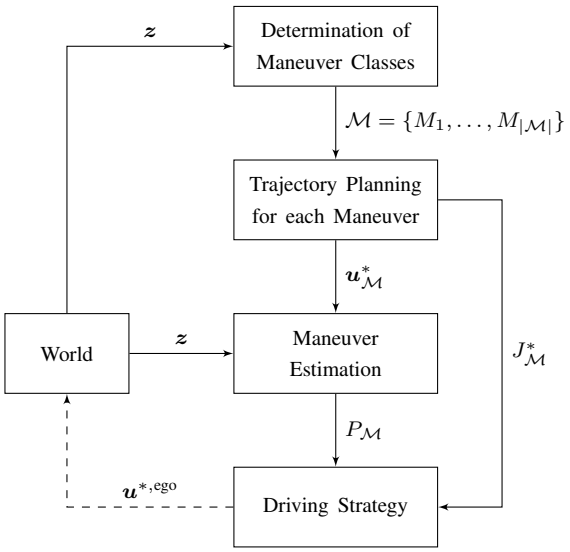

Fig. 2. Maneuver estimation and driving strategy framework. Dashed arcs represent temporal dependencies whereas solid arcs represent causal dependencies. The variables are defined in the corresponding sections.

sheer in. For intersections, many previous works have tried to predict the outgoing lane vehicles are going to take [3]–[8]. For that purpose, maneuvers of type *turn right*, *turn left* or *go straight* have been defined.

Another way of defining maneuvers is to cluster paths or trajectories into homotopy classes, which has already been used in the area of robotics for ego-vehicle motion planning [9]–[16]. Kuderer et al. [14] present an online framework to generate homotopically distinct navigation paths with the help of Voronoi diagrams. By using homotopy classes they avoid sticking to local minima during the path optimization. Bender et al. [16] propose to distinguish different maneuvers of autonomous vehicles with nearby dynamic obstacles based on homotopy classes and determine the best trajectory within those classes without the need of global optimization techniques. Gu et al. [15] automatically discover tactical maneuver patterns based on sampled trajectories. Using pseudo-homology, they can extract distinct maneuver classes and decide according to cost functions. All these works focus on ego-vehicle motion planning and assume other traffic participants to have known motion profiles such as constant velocity. Thus, these approaches are not suitable for maneuver prediction and only allow for single-agent environments, neglecting the fact that vehicles react to each other and their decisions may be coupled.

For the actual estimation of the intended maneuver given available observations, there are many different methods, reaching from discriminative models like SVMs [17] to probabilistic discriminative models like CRFs [8] to probabilistic generative models like Bayesian networks or HMMs [2]–[6]. Although some of those works explicitly model interactions between vehicles within their behavior models, their maneuver representations still lack the descriptive power to specify the relative motion of vehicles in detail, beneficial for scenarios with close interaction between vehicles.

III. Maneuver Determination

In this section, a collective maneuver representation for multi-agent systems based on trajectory homotopy is proposed and it is shown how a set of possible maneuvers can be derived given a traffic scenario with lane-precise map data. Within the scope of this paper, the desired exit direction of a vehicle crossing an intersection is assumed to be known.

A. Multi-Agent System

1) Trajectory: Assume a set of vehicles $\mathcal{V} = \{V_1, \cdots, V_N\}$ including the ego-vehicle is considered within the multi-agent system. The state of vehicle $V_n \in \mathcal{V}$ is given by $\boldsymbol{x}^n = [s^n, v_s^n, d^n, v_d^n]^\top \in \mathbb{R}^4$, consisting of the longitudinal and lateral Frenét-coordinates [18] s^n and d^n of the vehicle's center-position and the corresponding velocities $v_{s/d}^n$. The area occupied by this agent is approximated with a bounding box with length l^n and width w^n oriented along the tangent of the road's centerline: $\mathbb{A}(s^n, d^n, l^n, w^n) := \mathbb{A}^n \subset \mathbb{R}^2$. Changes in orientation, e.g. during lane changes, are neglected. Furthermore, the area occupied by static obstacles is denoted as $\mathbb{O} \subset \mathbb{R}^2$. The multi-agent configuration is defined as

$$\boldsymbol{x} = [\boldsymbol{x}^1, \cdots, \boldsymbol{x}^N]^\top \in X \subset \mathbb{R}^{4N} \tag{1}$$

within the collision-free configuration space

$$X = \{\boldsymbol{x} \mid \forall n, m \in \{1, \cdots, N\}, n \neq m: \\ (\mathbb{A}^n \cap \mathbb{O} = \emptyset) \wedge (\mathbb{A}^n \cap \mathbb{A}^m = \emptyset)\}. \tag{2}$$

On the basis of [16] for single agent trajectories, we define a multi-agent-trajectory to be a mapping from time span to configuration space: $\gamma : [0, T] \to X$.

2) Formation: To describe the relative order of the different agents within a multi-agent configuration $\boldsymbol{x}$ in an abstract way, the *formation* $F(\boldsymbol{x})$ is extracted. Any formation F holds information about the two dimensional relative position of objects, neglecting the exact distances and lengths. This allows for a compact description of the maneuver relevant aspects of the current scene.

For every street section without intersections, a local Frenét coordinate system is defined. The two dimensional positions of all vehicles on this section are first projected onto the longitudinal dimension. All vehicles are sorted in a list in ascending order according to s^n, storing the sequence of vehicles along the section. This list is then extended to a second dimension using the discrete lane matching information, resulting in the formation for that section (see Fig. 3(a)). Each cell within a formation is at most occupied by one vehicle, two vehicles cannot be on the same longitudinal column, i.e. laterally adjacent cells of an occupied cell are always unoccupied. Although in reality vehicles might overlap, it is not stored in the formation as it is not needed for the determination of the possible maneuvers.

Using map data, it is possible to extract the different sections and how they are connected at intersections. The formations of the single sections are derived independently and then linked using intersection cells (Fig. 3(b)). If lanes

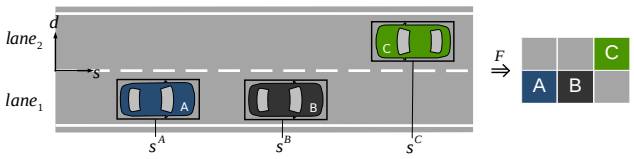

(a) Formation of a section using a local Frenét coordinate system and lanes.

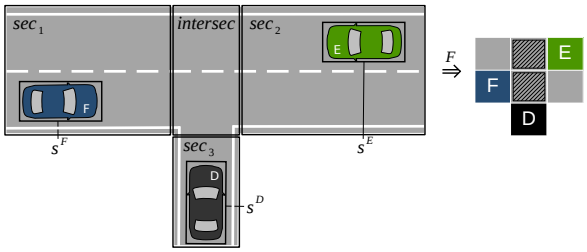

(b) Formations of multiple sections are connected using intersection cells.

Fig. 3. Derivation of the formation $F(\boldsymbol{x})$ of a given configuration $\boldsymbol{x}$.

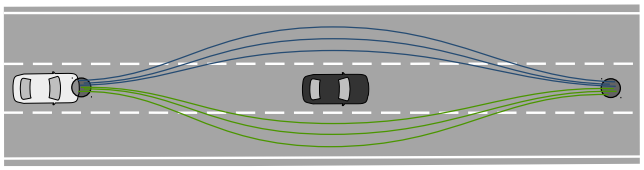

Fig. 4. Single-agent path homotopy: All paths of same color are homotopic relative to the start and end position areas (gray circles).

of an intersection overlap, they share at least one common cell. If a vehicle is currently driving on an intersection, the formation will relocate the vehicle to the connecting lane of the subsequent normal section and queue it behind all other vehicles, hence, intersection slots are never occupied.

B. Homotopy Classes

1) General Homotopy: In the field of topology, two functions $g_1, g_2 : Q \to R$ are said to be homotopic (or to be in the same homotopy class), if it is possible to *continuously deform* one into the other [13]. Hence a continuous homotopy $H : Q \times [0,1] \to R$ has to exist, such that

$$H(q,0) = g_1(q) \quad \wedge \quad H(q,1) = g_2(q) \quad \forall q \in Q. \tag{3}$$

Furthermore, g_1 and g_2 are called homotopic relative to the subspace $\tilde{Q} \subset Q$, if they are homotopic and

$$H(\tilde{q},\lambda) = g_1(\tilde{q}) = g_2(\tilde{q}) \quad \forall \tilde{q} \in \tilde{Q} \wedge \forall \lambda \in [0,1]. \tag{4}$$

2) Single-Agent Path Homotopy: In the case of robot motion planning, path homotopies are usually defined relative to the paths' start and end positions [10], [14]. Typically, the start position is known and it is desired to distinguish different end positions and whether obstacles are passed on the left or right side. To allow for inaccuracy in planning, this condition is often relaxed such that the start and end positions only need to be in specific areas. This is illustrated in Fig. 4. Without keeping the start and end positions in fixed areas, it would be possible to continuously deform all paths into each other. Hence, no distinction between passing the obstacle on the left or right side could be made.

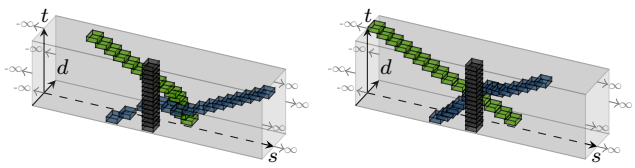

Fig. 5. Multi-agent trajectory homotopy: Two non-homotopic multi-agent trajectories of the scene of the left part of Fig. 1 are shown. On the left, V_A (blue) passes V_B (black) first, then V_C (green), on the right the other way around. Considering road boundaries and planning horizon to be obstacles of infinite size, different homotopy classes can be defined relative to the start and end formation.

3) Multi-Agent Trajectory Homotopy: Similar to [12] and [15], we extend the concept of path homotopy to the area of trajectories by adding the dimension of time and introducing the following assumptions for structured environments: First, the constraint of keeping start and end states at fixed positions or areas is relaxed to keeping them within fixed formations. Secondly, road boundaries and the planning horizon are interpreted as obstacles of infinite size, as shown in Fig. 5. Hence, it is not possible for a trajectory to run outside the road boundaries or beyond the planning horizon.

For two multi-agent trajectories to be homotopic, the trajectories of all vehicles need to allow a continuous transformation without colliding with obstacles or each other. Two mulit-agent trajectories $\gamma_0, \gamma_1 : [0,T] \to X$ with the same start and end formation $F(\gamma_0(0)) = F(\gamma_1(0)) := F_0$ and $F(\gamma_0(T)) = F(\gamma_1(T)) := F_T$ are said to be homotopic relative to $\{F_0, F_T\}$, if there exists a continuous homotopy $H : [0,T] \times [0,1] \to X$, such that

$$H(t,0) = \gamma_0(t) \quad \wedge \quad H(t,1) = \gamma_1(t) \quad \forall t \in [0,T] \tag{5}$$

and

$$F(H(0,\lambda)) = F_0 \ \wedge \ F(H(T,\lambda)) = F_T \quad \forall \lambda \in [0,1]. \tag{6}$$

In addition to the lateral sides agents pass each other, trajectory homotopy also considers temporal aspects: Consider the scenario in Fig. 5 with a laterally bounded street such that at most two vehicles can be next to each other. Given the start and end formation, both V_A and V_C have to pass V_B. As at the longitudinal occupancy of V_B there is only space for one other vehicle, different *sequences* in which V_B is passed need to be distinguished. As it is impossible to continuously transform the trajectories of Fig. 5 (left) to those of Fig. 5 (right), they belong to different homotopy classes.

4) Pseudo Multi-Agent Trajectory Homotopy: Except for the start and end formations, the trajectory homotopy defined previously is solely based on the multi-agent configuration including the areas of obstacles and agents, but not on high level information such as lanes. Consider the same scenario depicted in Fig. 5, but assume that geometrically, there is enough space for all three vehicles to be on the same longitudinal position. As drivers tend to drive on lanes, typical behavior for V_A would still include a discrete decision to either overtake before V_C or after. With trajectory homotopy, it is not possible to distinguish these two maneuvers, as it is possible to continuously deform one into the other. The same is true for three or more adjacent lanes.

Therefore, we propose a pseudo homotopy based on formations, that combines the advantages of homotopy with additional domain knowledge. The following spatial and temporal relations allow a high-level description of the relative motion in a comprehensible way that can be used to distinguish maneuvers. First of all, if two longitudinally adjacent vehicles pass each other, the side on which they do is of interest. This is denoted as *pairwise lateral relations* and can be derived by the discrete lane matchings. In many situations, the temporal order in which vehicles pass a specific area is of importance. This area might either be on an intersection, where vehicles have to pass sequentially, or on a normal section where there are conflicts on a lane such as in the example above. This temporal order is denoted as *sequence of passing* of that critical area.

A maneuver $M_i \in \mathcal{M}$ is given by a series of consecutive formations from F_0 to F_{Ti}, including all *pairwise lateral relations* and all *sequences of passing* of the critical areas, and represents one pseudo trajectory homotopy class.

C. Formation Tree

As this paper focuses on the prediction of human drivers, we are not only interested in the one optimal homotopy class, but in all possible reasonable classes that human drivers might choose. To determine the set of possible maneuvers in every time step, first the current formation F_0 of a given scene is identified using the positions of all considered vehicles and the available map data. Building a formation tree with root node F_0 and expanding it iteratively, different possible end formations F_{Ti} together with the corresponding intermediate formations can be found.

1) Expansion: The relative motion between agents is described on high abstraction level using a set of discrete actions $\mathcal{A} = \{a_{\text{long}}, a_{\text{left}}, a_{\text{right}}\}$ vehicles can choose from. The actions do not represent continuous motion, but changes in the relative order. A vehicle-action-pair $(V, a) \in \mathcal{V} \times \mathcal{A}$ transforms one formation into another. The vehicle that is in the longitudinal sequence of vehicles next in driving direction, independently of the lane, is from now on abbreviated as the *vehicle ahead*. The lateral actions a_{left} and a_{right} represent lane changes whereas the longitudinal action a_{long} can represent two things: passing the vehicle ahead, resulting in a switch of their longitudinal order, or passing an intersection and queuing into the connecting lane on the subsequent normal section. Intersection cells only serve as a connection between regular cells and are never occupied within a formation.

For any vehicle-action-pair $(V, a) \in \mathcal{V} \times \mathcal{A}$ and a given formation F_i, a new formation F_i' can be derived. See Fig. 6(a) for an example of how the formation changes for the different possible vehicle-action-pairs. Different tuples can in fact result in the same new formation, the relative motion is expressed on a multi-agent scale (e.g. in the formation on top of Fig. 6(a), $(V_{\text{B}}, a_{\text{long}})$ results in the same new formation as $(V_{\text{C}}, a_{\text{long}})$). Through exhaustive expansion by checking all possible actions of all vehicles, the tree can be built up gradually.

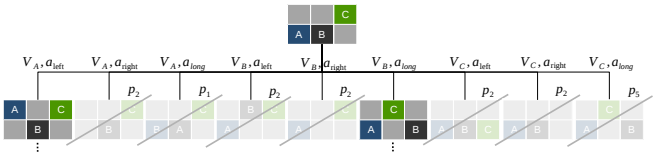

(a) First iteration of the maneuver expansion tree, showing how vehicle-action-pairs transform one formation to another. Formations that are pruned due to the pruning conditions $p_i \in \mathcal{P}$ are crossed out.

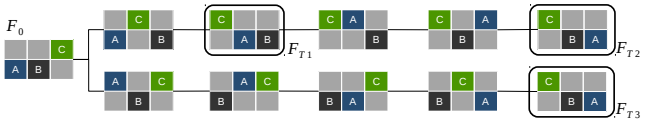

(b) Three possible maneuvers M_1, M_2, M_3 consisting of the sequences from F_0 to F_{T1} (V_{A} *follows* V_{B}), F_{T2} (V_{A} *overtakes* V_{B} *before* V_{C} passes V_{B}) and F_{T3} (V_{A} *overtakes* V_{B} *after* V_{C} has passed V_{B}).

Fig. 6. Formation tree expansion to identify reasonable maneuvers.

2) Pruning: The *pruning conditions* $\mathcal{P}$ are used exclude the occurrence of loops and unfeasible or unlikely behavior:

- p_1: *Passing on same lane*: passing the vehicle ahead if it is on the same lane
- p_2: *Unsuitable lane change*: changing to the lane of the vehicle ahead if it is oncoming;
  performing a lane change to a non existing lane
- p_3: *Reverse lateral action*: changing to a lane previously driven on within this maneuver, without having overtaken another vehicle
- p_4: *Re-overtaking*: two vehicles passing each other that have previously passed each other within this maneuver
- p_5: *Existing new formation*: a new formation that already exists having the same parent formation

These heuristics do not consider reasonable vehicle dynamics as a prerequisite yet, but this will be part of future work to further reduce complexity.

3) Final formation: A sequence of consecutive formations is only considered to be a valid maneuver if its final formation meets the *final formation conditions* $\mathcal{F}$:

- f_1: all vehicles with different driving directions have passed each other
- f_2: all vehicles are on a lane with correct driving direction

The expansion process is continued even on possible final formations until no new formations can be found anymore. A graphical representation of a maneuver search tree including the possible final formations is shown in Fig. 6(b).

4) Removing Duplicates: It is possible that multiple maneuvers in the tree are similar in a way no distinction is desired. As an example, consider two vehicles crossing an intersection using lanes that do not overlap (i.e. using different intersection cells). Then the temporal order in which they cross that intersection is not of importance. Similarly on normal sections, consider four vehicles $V_1 - V_4$ driving successively. If V_1 passes V_2 and V_3 passes V_4, the order in which these two actions happen is not of interest. Similar maneuvers like those are united, and the corresponding constraints are left out for the trajectory planning.

IV. Trajectory Planning

To allow for a comparison of abstract maneuver classes and an observed trajectory, we suggest to represent any abstract maneuver class by (at least) one multi-agent *sample estimate* trajectory. Assuming this trajectory reflects common driver behavior for that maneuver, it is possible to infer the probability distribution over the possible maneuvers by comparing the sample trajectories to the observed motion.

To generate a reasonable sample trajectory for every maneuver, an optimization problem is formulated that aims to minimize a collective cost-function while satisfying the hard constraints given by the specific maneuver class. Similar to [19], mixed-integer quadratic programs with logical constraints are used to enforce specific maneuvers.

A. State-Space Model

Since the purpose of the motion model is to determine a maneuver estimate rather than to generate smooth trajectories, it is represented by a simple double integrator, assuming the longitudinal and lateral acceleration $\boldsymbol{u}^n = [a_s^n, a_d^n]^\top$ of vehicle V^n can be controlled directly. For such a separated motion model, the side slip angle $\beta = \arctan(v_d/v_s)$ can be limited to allow the trajectories to be followed by non-holonomic vehicles [20].

The multi-agent trajectory γ can be derived with the initial state $\boldsymbol{x}_0$ and the sequence of control inputs $\boldsymbol{u}(k) = [\boldsymbol{u}^1(k), \cdots, \boldsymbol{u}^N(k)]^\top \quad \text{with} \quad k \in \{0, \cdots, K-1\}$. The motion models of the single vehicles are independent given their control inputs. However, their control inputs are coupled through the multi-agent optimization which accounts for the interdependencies between vehicles.

B. Hard Constraints

Independently of the maneuver, the state and control variables of all vehicles are bounded to ensure reasonable vehicle dynamics. Furthermore, vehicles are constrained to stay within the road boundaries. These maneuver-independent constraints are denoted as $\mathcal{C}$.

To enforce the planned trajectory to lie within the range of the given maneuver M_i, restricting the planning space to a specific pseudo-homotopy class, maneuver-dependent constraints $\mathcal{C}_{M_i}$ are formulated. As explained in Sec. III, maneuvers distinguish between spatial conditions (i.e. on which side two vehicles pass each other) and temporal conditions (i.e. in which order vehicles pass a critical area).

1) Spatial Collision Avoidance: Consider any pair of two vehicles V_A and V_B within a multi-agent environment, approximated by rectangles with length l and width w oriented along the centerline of a two-lane road. The spatial collision avoidance of V_A and V_B, i.e. interdicting any overlapping but not stating whether they pass each other or on which side, can be enforced by:

$$\begin{aligned}&(s^\mathrm{A} \leq s^\mathrm{B} - l) \vee (s^\mathrm{A} \geq s^\mathrm{B} + l)\\ \vee &(d^\mathrm{A} \leq d^\mathrm{B} - w) \vee (d^\mathrm{A} \geq d^\mathrm{B} + w)\end{aligned} \tag{7}$$

Additional safety distances can easily be incorporated by adding or subtracting the desired margin respectively.

Constraints of that nature are called logical constraints, as they combine linear constraints using logical operators. With the use of the so-called *Big M method* [21], [22], those logical constraints can be reformulated into a set of linear inequality constraints. By introducing an application-specific big number M^big, single conditions can be rendered inactive by the addition or subtraction of M^big depending on the value of a binary variable δ_i. This binary variable states whether the condition is active ($\delta_i = 1$) or not ($\delta_i = 0$). The logical disjunction of single binary variables is equivalent to at least one of the corresponding conditions to be active:

$$s^\mathrm{A} \leq s^\mathrm{B} - l + (1-\delta_1)M^\mathrm{big} \tag{8}$$
$$s^\mathrm{A} \geq s^\mathrm{B} + l - (1-\delta_2)M^\mathrm{big} \tag{9}$$
$$d^\mathrm{A} \leq d^\mathrm{B} - w + (1-\delta_3)M^\mathrm{big} \tag{10}$$
$$d^\mathrm{A} \geq d^\mathrm{B} + w - (1-\delta_4)M^\mathrm{big} \tag{11}$$
$$\delta_1 + \delta_2 + \delta_3 + \delta_4 \geq 1 \tag{12}$$

The *pairwise lateral relations* specified by a maneuver can be enforced using these spatial conditions by setting the corresponding binary variable (either δ_3 or δ_4) to 0.

2) Temporal Collision Avoidance: Now consider the scenario depicted in Fig. 5 with the three vehicles V_A, V_B, V_C. Additionally to the conditions for the *pairwise lateral relations*, a desired *sequence of passing* (e.g. V_A before V_C) can be enforced by the temporal condition

$$(s^\mathrm{C} \leq s^\mathrm{B}) \Rightarrow (s^\mathrm{A} > s^\mathrm{B}). \tag{13}$$

This can be reformulated in Big M notation as

$$s^\mathrm{C} > s^\mathrm{B} - \delta_k M^\mathrm{big} \tag{14}$$
$$s^\mathrm{A} > s^\mathrm{B} - (1-\delta_k)M^\mathrm{big}, \tag{15}$$

thus, only one additional binary variable is needed to enforce the desired sequence.

3) Separation of Longitudinal and Lateral Optimization: To reduce the number of needed binary variables and hence reduce complexity, the problem is divided into two subproblems: optimizing the longitudinal and lateral control inputs separately. In the field of single-agent planning, this has already been suggested by [23]. The longitudinal optimization ensures the correct *sequences of passing*, whereas the lateral optimization ensures the correct *pairwise lateral relations*. By first solving the longitudinal optimization, its results can be used as an input for the lateral part. Hence, for the lateral optimization, the longitudinal positions of all vehicles are known in advance. The spatial collision avoidance constraints can thus be expressed without the need of binary variables. For the aforementioned overtaking scene, the number of binary variables is reduced from ten (three per *pairwise lateral relation* and one for the *sequence of passing*) to one per time step. Furthermore, as the values of the single δ_i are known for $k = 0$, motion is only allowed within driving direction and re-overtaking is forbidden, the single binary variables can change their values at most once during one maneuver. Hence the number of possible combinations per binary variable reduces from 2^K to $(K+1)$.

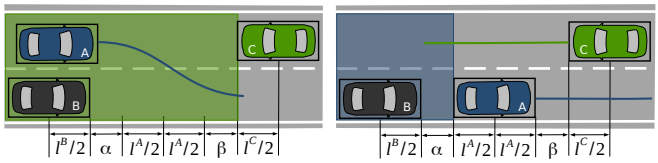

Fig. 7. Longitudinal constraints for maneuver M_2 to enforce a desired *sequence of passing*. On the left, equation (16) is active ($\delta_1 = 0$) and V^{C} is not allowed to enter the green area. As soon as V^{A} has overtaken V^{B}, this restriction is removed and equation (17) is activated ($\delta_1 = 1$).

The longitudinal constraints to enforce a desired *sequence of passing* are adapted by the typical length needed for a lane change α and a sufficient safety distance β. These distances are illustrated exemplarily for the maneuver M_2 in Fig. 7 (see Fig. 6(b) for maneuver definition). The longitudinal constraints (14) and (15) of M_2 change accordingly:

$$s^{\mathrm{C}} > s^{\mathrm{B}} + l^{\mathrm{B}}/2 + \alpha + l^{\mathrm{A}} + \beta + l^{\mathrm{C}}/2 - \delta_1 M^{\mathrm{big}} \tag{16}$$

$$s^{\mathrm{A}} > s^{\mathrm{B}} + l^{\mathrm{B}}/2 + \alpha + l^{\mathrm{A}}/2 - (1-\delta_1) M^{\mathrm{big}} \tag{17}$$

The constraints of M_3 are defined analogously, the ones for M_1 only contain a safety distance between V_{A} and V_{B}. For intersection scenarios, the longitudinal constraints are defined relative to the overlapping areas.

The state and the control inputs as well as the optimization constraints, the cost function and its weights can be divided into a longitudinal and a lateral part, which are from now on denoted by subscript s and d, respectively.

C. Cost-Function

For the trajectories to reflect common human behavior, a quadratic cost-function is chosen that penalizes acceleration as well as the deviation from the desired speed and the desired lateral position. The deviation of state and reference state $\boldsymbol{x}^{n,\mathrm{ref}} = [s^{n,\mathrm{ref}}, v_s^{n,\mathrm{ref}}, d^{n,\mathrm{ref}}, v_d^{n,\mathrm{ref}}]^\top$ is given by

$$\Delta \boldsymbol{x}_k^n = \boldsymbol{x}_k^n - \boldsymbol{x}_k^{n,\mathrm{ref}}. \tag{18}$$

The value of $v_s^{n,\mathrm{ref}}$ represents the desired speed v_s^{des}, $v_d^{n,\mathrm{ref}}$ is zero, and $d^{n,\mathrm{ref}}$ is the center of the current lane. The value of $s^{n,\mathrm{ref}}$ is irrelevant, as the corresponding weight is zero.

The collective cost function of the multi-agent optimization problem is defined quadratic w.r.t. the control inputs as well as the deviation of state and reference state as

$$J = J_s + J_d = \sum_{n=1}^{N} J_s^n + \sum_{n=1}^{N} J_d^n, \tag{19}$$

with the components of the single vehicles

$$J_s^n = \sum_{k=1}^{K} (\Delta \boldsymbol{x}_{s,k}^n)^\top \boldsymbol{Q}_s^n \Delta \boldsymbol{x}_{s,k}^n + \sum_{k=0}^{K-1} u_{s,k}^n R_s u_{s,k}^n, \tag{20}$$

$$J_d^n = \sum_{k=1}^{K} (\Delta \boldsymbol{x}_{d,k}^n)^\top \boldsymbol{Q}_d^n \Delta \boldsymbol{x}_{d,k}^n + \sum_{k=0}^{K-1} u_{d,k}^n R_d u_{d,k}^n. \tag{21}$$

By taking the costs of other vehicles into account, drivers are assumed to behave cooperatively. The state weighting matrices $\boldsymbol{Q}_s^n = \mathrm{diag}(0, \omega)$ and $\boldsymbol{Q}_d^n = \mathrm{diag}(\omega, \omega/2)$ and the control input weights $R_s^n = \omega$ and $R_d^n = \omega/2$ are chosen by expert knowledge. The weight $\omega = 1 + (\gamma - 1)\rho$ depends on whether a vehicle has right of way ($\rho = 1$) or not ($\rho = 0$) and on how strong drivers weigh these traffic rules (γ). This encourages traffic rule compliance in a soft manner, still allowing drivers to slightly deviate if necessary.

The longitudinal optimization for maneuver M_i can be formulated as

$$[\boldsymbol{u}_{s,M_i}^*, \boldsymbol{\delta}^*]^\top = \underset{[\boldsymbol{u}_s, \boldsymbol{\delta}]^\top}{\arg\min}\, J_s \quad \text{subject to} \quad \mathcal{C}_s \cup \mathcal{C}_{M_i,s}, \tag{22}$$

resulting in the optimal longitudinal costs $J_{M_i,s}^*$. After determining $\boldsymbol{u}_{s,M_i}^*$, the QP for the lateral optimization can be defined only using linear inequality constraints as

$$\boldsymbol{u}_{d,M_i}^* = \underset{\boldsymbol{u}_d}{\arg\min}\, J_d \quad \text{subject to} \quad \mathcal{C}_d \cup \mathcal{C}_{M_i,d}, \tag{23}$$

resulting in the optimal lateral costs $J_{M_i,d}^*$. Note that only the hard constraints depend on the specific maneuver M_i, whereas the cost-function is maneuver-independent. The overall optimal costs of M_i are determined by the sum of the optimal costs of both the longitudinal and lateral component:

$$J_{M_i}^* = J_{M_i,s}^* + J_{M_i,d}^* \tag{24}$$

The trajectory planning with the corresponding hard constraints is exemplarily depicted for an overtaking scenario in Fig. 8. Within this example, only V_{A} and V_{C} are considered within the multi-agent planning, V_{B} is considered to be parked. The cost-optimal trajectory of each of the three possible maneuver hypotheses are shown (M_1: *follow*, M_2: *overtake before oncoming*, M_3: *overtake after oncoming*).

V. Maneuver Estimation

Any driver is assumed to have exactly one intended maneuver at a given time step. The intended maneuver can switch between time steps, which satisfies the fact that drivers continuously re-evaluate situations and may change their intentions. Thus, the motion of vehicles is modeled as a stochastic process that consists of $|\mathcal{M}|$ different models, exactly one being active per time step. Following [4], the maneuver switching probability is set to $\mu = 0.1$ and distributes uniformly among all other maneuvers.

The prediction task is to estimate the active model from which the drivers choose their actions. This is achieved by an interacting multiple model (IMM) Kalman filter. The prediction steps of maneuver M_i are performed according to the controls $\boldsymbol{u}_{M_i}^*$ of the optimal trajectory. Through Bayesian statistics, the posterior mode probabilities $\boldsymbol{P}_{\mathcal{M}} = [P_{M_1}, \cdots, P_{M_{|\mathcal{M}|}}]^\top$ are obtained in every time step given the predicted states, the measurement of the positions $\boldsymbol{z} = [s_z^1, d_z^1, \cdots, s_z^N, d_z^N]^\top$, the last posterior and the switching probabilities. Initially, a uniform prior is assumed. For the determination of the single distributions, we refer to [24].

Although drivers may deviate from the sample trajectory of their intended maneuver, it is still possible to estimate the maneuver correctly, as long as the deviation is smaller compared to the sample trajectories of the other maneuvers. An exemplary probability distribution of a given scene is depicted in Fig. 8(d).

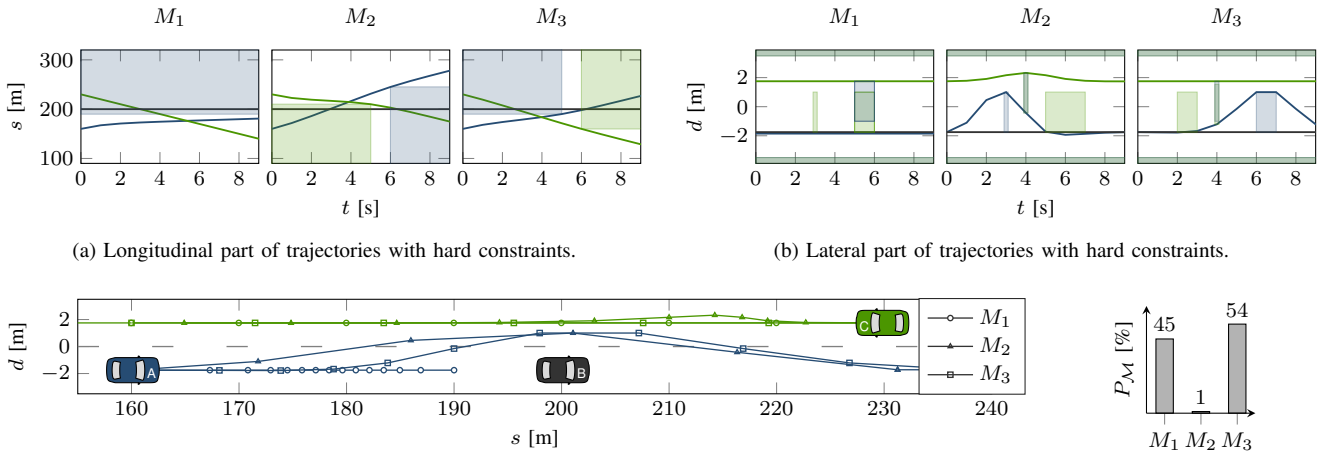

(a) Longitudinal part of trajectories with hard constraints.

(b) Lateral part of trajectories with hard constraints.

(c) Optimal trajectories of all considered maneuvers.

(d) IMM maneuver probabilities.

Fig. 8. Overtaking scenario with oncoming traffic: Multi-agent trajectories for all maneuvers in $\mathcal{M}$ and resulting maneuver probability distribution $P_{\mathcal{M}}$. The colors of the trajectories (lines) and the hard constraints (areas) correspond to the vehicles' colors. The hard constraints constrain the trajectories due to the road boundaries and other vehicles: the trajectories are not allowed to be inside the areas of same color.

To close the loop of the prediction and planning framework (see Fig. 2), a simple driving strategy is applied, that decides for the most likely maneuver according to $\boldsymbol{P}_{\mathcal{M}}$. The ego-vehicle is then controlled according to the accelerations $\boldsymbol{u}^{*,\text{ego}}$ of the corresponding optimal trajectory.

VI. Experiments

The maneuver estimation capabilities of our IMM approach is compared to a trajectory-cost-based classification and a cost-gradient-based classification, inspired by [25]. In the latter two approaches, the ego-vehicle decides for the maneuver M_i with the lowest optimal cost $J^*_{M_i}(k)$ and lowest optimal cost-gradient $\Delta J^*_{M_i}(k) = J^*_{M_i}(k) - J^*_{M_i}(k-1)$, respectively, whereas our approach for the one with highest probability $P_{M_i}(k)$. Within the closed-loop simulation framework the desired maneuver of the non-ego-vehicles can be set a priori. All vehicles are controlled with receding horizon control according to the optimal trajectories of the given maneuver. Gaussian noise with variances according to Tab. I is added to the transition model and measurements.

The two scenarios in Fig. 1 are statistically evaluated. For the *overtaking* scenario, the maneuvers M_1, M_2 and M_3 have been determined, with V_C being the ego-vehicle, V_A being predicted and V_B having constant velocity. For the *merging* scenario, two maneuvers are distinguished: V_D merges before V_E (M_4) and V_D merges after V_E (M_5). V_E is the ego-vehicle whereas V_D is predicted. All parameters used for the evaluation are chosen by domain knowledge and are shown in Tab. I. To reflect different situations, the initial conditions consisting of desired velocities and initial positions of all vehicles are altered iteratively. Each run consists of 14 seconds and is repeated five times with the same initial conditions for each possible maneuver intention, generating the same number of sample points per maneuver.

The execution of one time step of the overtaking scenario including maneuver determination (*C++*), multi-agent trajectory planning and IMM update (*MATLAB*) takes approximately 0.26 s on an *Intel Core i7-4910MQ* with 2.9 GHz without code optimization or parallelization.

TABLE I
Parameters used for Evaluation

T	14 s	l	5 m	σ_s^2	1 m^2
ΔT	1 s	w	1.75 m	σ_d^2	0.1 m^2 s^{-2}
a_s	$[-9, 5]$ m s^{-2}	v_s^des	10 m s^{-1}	$\sigma_{v_s}^2$	0.25 m^2
a_d	$[-2, 2]$ m s^{-2}	α	2.5 m	$\sigma_{v_d}^2$	0.01 m^2 s^{-2}
v_s	$[0, 20]$ m s^{-1}	β	30 m	$\sigma_{z_s}^2$	5 m^2
v_d	$[-5, 5]$ m s^{-1}	γ	2	$\sigma_{z_d}^2$	5 m^2
v_des	30 m s^{-1}	μ	0.1		

Fig. 9 depicts the IMM maneuver probabilities depending on the tracking time steps with the maneuver intention set to *follow* (i.e. ground truth is M_1). Although maneuver *follow* and *overtake after* (M_3) have similar optimal trajectories, they can still be distinguished after about three time steps. The confusion matrices given in Tab. II show a quantitative comparison of the actual maneuver and the estimates of the different estimators for time steps $1-14$ for the cost-based estimator and $2-14$ for the other estimators. The results show for both overtaking (left part) and merging (right part) that only relying on the costs often yields wrong maneuver estimates as the simulated vehicles randomly decide for a maneuver which is not necessarily the one with lowest costs. However, the costs of the intended maneuver tend to get smaller the longer the predicted vehicles follow their intentions, slightly improving the accuracy compared to a random classifier. One advantage of the cost-based estimation is the instant assessment without having to wait for the subsequent time step. The cost-gradient estimator achieves better and faster results, as it uses two consecutive measurements and therefore is able to analyze the actual behavior instead of only a static situation. However, the cost-gradient completely neglects the absolute costs, sporadically resulting in even worse accuracies. The IMM estimator, using all available past measurements, outperforms the cost-based as well as the cost-gradient-based classification.

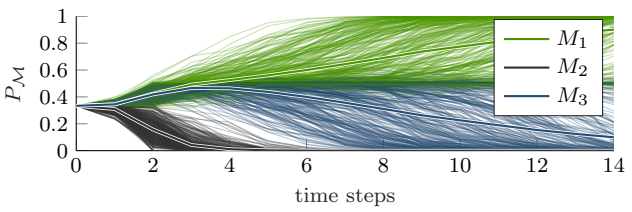

Fig. 9. IMM maneuver probabilities for the overtaking scenario with maneuver intention *follow*, i.e. ground truth M_1. The mean values of all runs with different initializations are drawn as lines with white boarders.

TABLE II
CONFUSION MATRICES FOR ESTIMATORS BASED ON J^*, ΔJ^* AND P

Actual	based on J^*			Acc	Actual	based on J^*		Acc
	M_1	M_2	M_3			M_4	M_5	
M_1	**746**	811	3393	0.15	M_4	**11112**	5763	0.66
M_2	312	**3833**	805	0.77	M_5	5660	**11215**	0.66
M_3	693	836	**3421**	0.69				**0.66**
				0.54				

Actual	based on ΔJ^*			Acc	Actual	based on ΔJ^*		Acc
	M_1	M_2	M_3			M_4	M_5	
M_1	**505**	517	3598	0.11	M_4	**13690**	2060	0.87
M_2	19	**4458**	143	0.96	M_5	2352	**13398**	0.85
M_3	546	526	**3548**	0.77				**0.86**
				0.61				

Actual	based on P			Acc	Actual	based on P		Acc
	M_1	M_2	M_3			M_4	M_5	
M_1	**3476**	60	1084	0.75	M_4	**15060**	690	0.96
M_2	20	**4539**	61	0.98	M_5	530	**15220**	0.97
M_3	825	84	**3711**	0.80				**0.96**
				0.85				

VII. CONCLUSION

In this paper, we presented a Bayesian collective maneuver estimation framework, based on trajectory homotopy and multi-agent planning. The maneuver representation is capable of describing the relative motion of multiple vehicles within a scene and can handle adjacent as well as intersecting or merging lanes. Our interacting multiple model approach outperforms the cost-based as well as the cost-gradient-based classification method in the tested scenarios. The calculated optimal trajectory of the most likely maneuver can directly be used as control input resulting in a closed-loop framework with a cooperatively driving autonomous vehicle.

Future work includes the evaluation on real world data as well as the adaptation of the trajectory planning parameters to better reflect real human behavior. It should be tested, how many sample trajectories per maneuver are sufficient to reflect the variance within different drivers. Different vehicle types and driving styles could also be modeled explicitly or learned from data.

REFERENCES

[1] M. Tsogas, X. Dai, G. Thomaidis, P. Lytrivis, and A. Amditis, "Detection of maneuvers using evidence theory," in *Intell. Veh. Symp. (IV)*, pp. 126–131, IEEE, 2008.

[2] T. Gindele, S. Brechtel, and R. Dillmann, "A probabilistic model for estimating driver behaviors and vehicle trajectories in traffic environments," in *Int. Conf. Intell. Transp. Syst. (ITSC)*, pp. 1625–1631, IEEE, 2010.

[3] M. Liebner, M. Baumann, F. Klanner, and C. Stiller, "Driver intent inference at urban intersections using the intelligent driver model," in *Intell. Veh. Symp. (IV)*, pp. 1162–1167, IEEE, 2012.

[4] S. Lefèvre, C. Laugier, and J. Ibañez-Guzmán, "Risk assessment at road intersections: Comparing intention and expectation," in *Intell. Veh. Symp. (IV)*, pp. 165–171, IEEE, 2012.

[5] S. Klingelschmitt, M. Platho, H.-M. Gross, V. Willert, and J. Eggert, "Combining behavior and situation information for reliably estimating multiple intentions," in *Intell. Veh. Symp. (IV)*, pp. 388–393, IEEE, 2014.

[6] F. Kuhnt, J. Schulz, T. Schamm, and J. M. Zöllner, "Understanding interactions between traffic participants based on learned behaviors," in *Intell. Veh. Symp. (IV)*, pp. 1271–1278, IEEE, 2016.

[7] D. Petrich, T. Dang, G. Breuel, and C. Stiller, "Assessing map-based maneuver hypotheses using probabilistic methods and evidence theory," in *Int. Conf. Intell. Transp. Syst. (ITSC)*, pp. 995–1002, IEEE, 2014.

[8] Q. Tran and J. Firl, "A probabilistic discriminative approach for situation recognition in traffic scenarios," in *Intell. Veh. Symp. (IV)*, pp. 147–152, IEEE, 2012.

[9] D. J. Demyen and M. Buro, "Efficient triangulation-based pathfinding," in *Assoc. for the Advancement of Artificial Intell. (AAAI)*, vol. 6, pp. 942–947, 2006.

[10] S. Bhattacharya, V. Kumar, and M. Likhachev, "Search-based path planning with homotopy class constraints," in *3rd Annu. Symp. Combinatorial Search*, 2010.

[11] B. Banerjee and B. Chandrasekaran, "A framework of voronoi diagram for planning multiple paths in free space," *J. Experimental & Theoretical Artificial Intell.*, vol. 25, no. 4, pp. 457–475, 2013.

[12] S. Bhattacharya, M. Likhachev, and V. Kumar, "Identification and representation of homotopy classes of trajectories for search-based path planning in 3d," 2011.

[13] S. Bhattacharya, M. Likhachev, and V. Kumar, "Topological constraints in search-based robot path planning," *Auton. Robots*, vol. 33, no. 3, pp. 273–290, 2012.

[14] M. Kuderer, C. Sprunk, H. Kretzschmar, and W. Burgard, "Online generation of homotopically distinct navigation paths," in *Int. Conf. Robot. Autom. (ICRA)*, pp. 6462–6467, IEEE, 2014.

[15] T. Gu, J. M. Dolan, and J.-W. Lee, "Automated tactical maneuver discovery, reasoning and trajectory planning for autonomous driving," in *Int. Conf. Intell. Robot. and Syst. (IROS)*, pp. 5474–5480, IEEE, 2016.

[16] P. Bender, O. S. Tas, J. Ziegler, and C. Stiller, "The combinatorial aspect of motion planning: Maneuver variants in structured environments," in *Intell. Veh. Symp. (IV)*, pp. 1386–1392, IEEE, 2015.

[17] P. Kumar, M. Perrollaz, S. Lefevre, and C. Laugier, "Learning-based approach for online lane change intention prediction," in *Intell. Veh. Symp. (IV)*, pp. 797–802, IEEE, 2013.

[18] M. Werling, J. Ziegler, S. Kammel, and S. Thrun, "Optimal trajectory generation for dynamic street scenarios in a frenet frame," in *Int. Conf. Robot. Autom. (ICRA)*, pp. 987–993, IEEE, 2010.

[19] X. Qian, F. Altché, P. Bender, C. Stiller, and A. De La Fortelle, "Optimal trajectory planning for autonomous driving integrating logical constraints: A MIQP perspective," in *Int. Conf. Intell. Transp. Syst. (ITSC)*, pp. 205–210, IEEE, 2016.

[20] J. Nilsson, M. Brännström, J. Fredriksson, and E. Coelingh, "Longitudinal and lateral control for automated yielding maneuvers," *IEEE Trans. Intell. Transp. Syst.*, vol. 17, no. 5, pp. 1404–1414, 2016.

[21] J. C. Smith and Z. C. Taskin, "A tutorial guide to mixed-integer programming models and solution techniques," *Optimization in Medicine and Biology*, pp. 521–548, 2008.

[22] J. Nocedal and S. Wright, *Numerical optimization*. Springer Science & Business Media, 2006.

[23] B. Gutjahr, C. Pek, L. Gröll, and M. Werling, "Efficient trajectory optimization for vehicles using quadratic programming," *Automatisierungstechnik*, 2016.

[24] Y. Bar-Shalom, P. K. Willett, and X. Tian, *Tracking and data fusion*. YBS publishing, 2011.

[25] A. von Eichhorn, M. Werling, P. Zahn, and D. Schramm, "Maneuver prediction at intersections using cost-to-go gradients," in *Int. Conf. Intell. Transp. Syst. (ITSC)*, pp. 112–117, IEEE, 2013.